Soils and Foundations ■■■;■(■):■■■–■■■

The Japanese Geotechnical Society

Soils and Foundations

www.sciencedirect.com
journal homepage: www.elsevier.com/locate/sandf

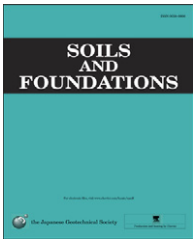

Stability of existing bridges improved by structural integration and nailing

Fumio Tatsuoka[a,*], Henry Muñoz[b], Tetsuya Kuroda[c], Hiroki Nishikiori[d], Ryoichi Soma[e], Takashi Kiyota[f], Masaru Tateyama[g], Kenji Watanabe[g]

[a]*Department of Civil Engineering, Tokyo University of Science (TUS), Chiba, Japan*
[b]*Japan-Peru Center for Earthquake Engineering Research and Mitigation of Disasters CISMID, National University of Engineering, Lima, Peru*
[c]*Tokyo Metropolitan Government, Japan*
[d]*Ibaraki Prefecture, Japan*
[e]*Toyo Engineering Co., Japan*
[f]*Institute of Industrial Science, University of Tokyo, Japan*
[g]*Structural Engineering Division, Railway Technical Research Institute, Japan*

Abstract

To examine whether and how the seismic stability of existing bridges can be substantially improved by integrating the girder, the abutments and the backfill, a series of shaking table tests were performed in 1 g. The tested small bridge models are (1) a conventional-type comprising a girder, supported by a pair of gravity-type abutments (without pile foundation) via bearings (fixed and movable), and unreinforced backfill, (2) the girder and the abutments of the above are integrated (without using bearings), (3) the backfill of the above is reinforced with two layers of large-diameter nails connected to the abutment top and the toe or the heel of the abutment footing and (4) the bottom nails of the above are replaced with longer ones connected to the toe of the abutment footing. Their dynamic behavior was analyzed as a damped single-degree-of-freedom system. The dynamic stability of the bridge was found to increase with an increase in (i) the dynamic strength against the response acceleration, (ii) the initial stiffness, (iii) the dynamic ductility (i.e., a smaller decreasing rate of stiffness during dynamic loading) and (iv) the damping ratio. When factors (ii) and (iii) are high enough, the natural frequency of a bridge can be kept much higher than the input frequency, and thus, the response acceleration can be kept low. All these factors can be improved by integrating the girder, the abutments and the backfill together with part of the supporting ground. In a series of static model tests, lateral cyclic displacements, caused by the seasonal thermal deformation of the girders with prototypes, were applied to the top of a small abutment model. The active failure in the backfill and the detrimental effects of large passive pressure, both developing due to the dual ratchet mechanism, can be effectively restrained by reinforcing the backfill and supporting the ground with nails connected to the top and the bottom of the abutments.

Keywords: Bridge abutment; Dynamic response; Integrated bridge; Model test; Nailing; Reinforcement; Seismic design (**IGC**: E-8/E-14/H-0)

1. Introduction

Conventional-type bridges usually comprise a single girder, simply supported by a pair of abutments via a pair of movable and fixed bearings, or multiple girders, simply supported by a pair of abutments and a pier (or piers) via multiple sets of bearings and connected with expansion joints. The backfill is unreinforced. A great number of conventional bridges collapsed during many previous earthquakes. Therefore, there is a strong need for a new cost-effective type of bridge that is much more earthquake-

*Corresponding author.
E-mail address: tatsuoka@rs.noda.tus.ac.jp (F. Tatsuoka).

Peer review under responsibility of The Japanese Geotechnical Society
http://dx.doi.org/10.1016/j.sandf.2012.05.004

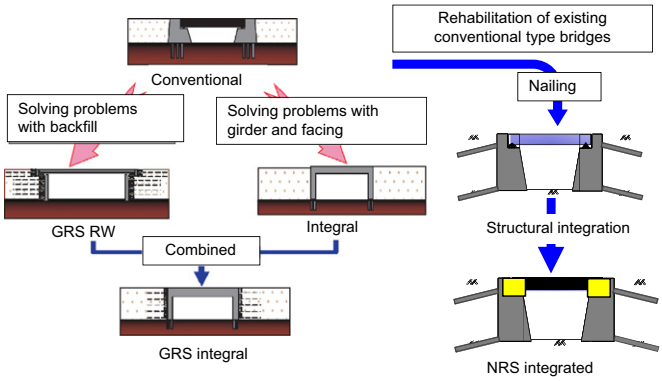

Fig. 1. Bridge types to alleviate technical problems with conventional type bridges (adapted from Tatsuoka et al., 2009).

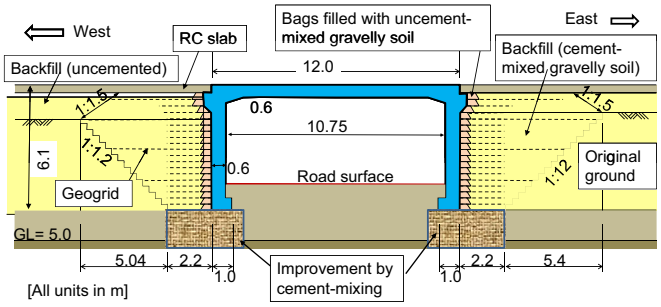

Fig. 2. First prototype GRS integral bridge (the width = 11.7 m), at Kikonai for a new bullet train line, the south end of Hokkaido (by the courtesy of the Japan Railway Construction and Technology Agency).

resistant. Tatsuoka et al. (2009) proposed a geosynthetic-reinforced soil (GRS) integral bridge for new construction, which is a combination of the conventional integral bridge (with unreinforced backfill) and the GRS retaining wall (RW) bridge (Fig. 1). That is, GRS integral bridges have no bearing to support the girder; the girder is continuous and the backfill is reinforced with geosynthetic reinforcement layers connected to full-height rigid (FHR) facings (i.e., the abutments). The FHR facings are constructed ensuring a strong connection to the wall face wrapped around with geosynthetic reinforcement layers after sufficient deformation of the reinforced backfill and the subsoil has taken place (Tatsuoka et al., 1997). As the FHR facing is not a cantilever structure, its structure is substantially lighter than the abutments of conventional bridges and the need for pile foundations is much lower (Tatsuoka, 1992). Based on the results of a series of static cyclic lateral loading tests and shaking table tests on small models in 1 g of the four types of bridges depicted in Fig. 1 (i.e., conventional, integral, GRS RW and GRS integral), Tatsuoka et al. (2009, 2012) and Muñoz et al. (2012) reported the following:

(1) For conventional-type integral bridges with unreinforced backfill, large settlement by active failure may take place in the backfill and the abutment may be seriously damaged due to significantly increased passive earth pressure, both caused by the cyclic lateral displacements at the abutment top by seasonal thermal expansion and the contraction of the girder. On the other hand, GRS integral bridges are free from these problems for the following reasons. Firstly, the active failure in the backfill is restrained by reinforcement layers connected to the facing. Secondly, the facing behaves as a continuous beam supported by a number of supports (i.e., reinforcement layers) with a short span; therefore, the active displacement of the facing by large earth pressure is restrained and the internal forces inside the facing are kept small.

The dynamic stability of conventional-type bridges is generally very low, because the end of the girder that is supported by a movable bearing and the unreinforced backfill are particularly unstable against seismic loads. With conventional-type integral bridges (Fig. 1), part of this and other problems with conventional-type bridges can be alleviated by integrating the girder to the abutments. However, the seismic stability of the unreinforced backfill remains low. With GRS RW bridges (Fig. 1), a part of these problems can be alleviated by reinforcing the backfill with geosynthetic reinforcement layers connected to the back of the FHR (Tatsuoka et al., 2005). However, the problems when using bearings remain unsolved and the sill beams that support the girder via the bearings are not stable against seismic loads. With GRS integral bridges, on the other hand, the above problems that integral bridges and GRS RW bridges still have can be alleviated, while they take advantage of the superior features of these two bridge types. Therefore, GRS integral bridges are much more cost-effective in terms of construction and long-term maintenance under static and seismic loading conditions than the other types.

(2) The high dynamic stability of GRS integral bridges can be attributed to (i) a high initial natural frequency, (ii) a low decreasing rate in the natural frequency during dynamic loading (i.e., high dynamic ductility), (iii) high dynamic strength against response acceleration and (iv) a high energy dissipation capacity.

In 2011, the first prototype GRS integral bridge was constructed (Fig. 2). Watanabe (2011) reports that the construction costs for this GRS integral bridge were much lower than those of a box girder type of bridge (the most conventional solution in this case) or a GRS RW bridge supporting a girder at the top of the FHR facing via fixed and movable bearings (i.e., the latest technology before the introduction of the GRS integral bridge) (Tatsuoka et al., 2005). In the meantime, the authors proposed rehabilitating existing conventional-type bridges judged not to satisfy the seismic stability requirements according to the current design standards by taking advantage of the structural characteristics of GRS integral bridges (Shiranita et al., 2010). As illustrated on the right side in Fig. 1, the backfill and a part of the supporting ground are reinforced with large-diameter nails connected to the abutments and the

Please cite this article as: Tatsuoka, F., et al., Stability of existing bridges improved by structural integration and nailing. Soils and Foundations (2012), http://dx.doi.org/10.1016/j.sandf.2012.05.004

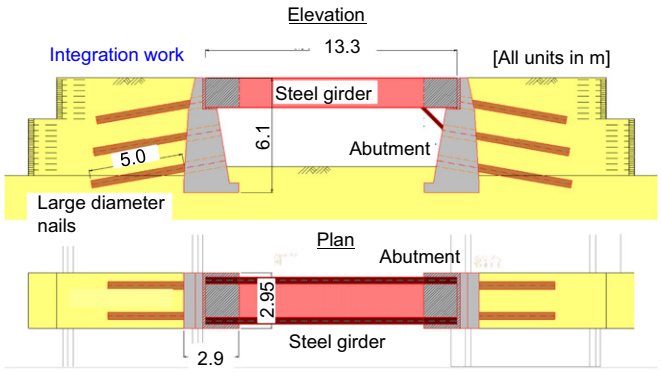

Fig. 3. Full-scale model of NRS integrated bridge (Suga et al., 2011).

girder is integrated to the abutments. The reinforced bridge is called a nail-reinforced soil (NRS) integrated bridge. To validate this proposal, a series of shaking table tests and static cyclic loading tests was performed on small models in 1 g. By the end of 2009, a full-scale model of a conventional-type bridge was constructed and the backfill at both sides was reinforced with 40-cm-diameter nails connected to the abutments; the steel girder was then integrated to a pair of abutments (Fig. 3; Suga et al., 2011). The high constructability of this bridge-reinforcement method was confirmed.

The first objective of the present study is to perform shaking table tests to examine whether and how the dynamic stability of NRS integrated bridges becomes considerably higher than that of original conventional-type bridges by similar mechanisms through which the GRS integral bridges become much more stable against dynamic loads (as described above). The second objective is to apply cyclic lateral displacements to the top of a model abutment, caused by the seasonal thermal deformation of the girder with prototypes, to examine whether and how the active failure in the backfill and the detrimental effects of the elevated passive pressure are effectively restrained with NRS integrated bridges.

2. Shaking table tests

Other than nailing the backfill and the supporting ground with large-diameter model nails, the method of the shaking table tests performed in the present study is the same as the one reported in detail by Tatsuoka et al. (2009) and Muñoz et al. (2012). Therefore, only a brief description is given here.

2.1. Bridge models

In total, six shaking table tests were performed in 1 g on small models of conventional-type bridges comprising a single simply supported girder and a pair of gravity-type abutments with unreinforced backfill (Fig. 4(a)) and conventional-type bridges reinforced in five different ways (Figs. 4(b)–(e)). The models were constructed inside a steel sand box (205.8 cm long, 60 cm wide and 140 cm high) fixed to a shaking table. The ratio in length between the conceived prototype and the small model, λ, is equal to 10. The front side of the sand box has a glass window, reinforced with steel stiffeners, to observe the models. The opposite side of the sand box comprises a steel plate covered with a 0.2-mm-thick Teflon sheet to minimize the wall friction. Yet, it is likely that the dynamic stability of the models may have been somehow over-estimated by small wall friction.

The results of these model tests may somehow be different from the behavior of the conceived prototype structures due to (a) pressure level effects and (b) particle size effects (i.e., effects of the ratio of particle size to model size) (e.g., Tatsuoka et al., 1991; Siddiquee et al., 1999; Tatsuoka, 2001). In the present study, the model test results were analyzed to understand the basic failure mechanism of, and the relative stabilities among, the different models. It is considered that they are not significantly different from those of the conceived prototypes, despite the possible effects of factors (a) and (b). The quantitative prediction of the behavior of the conceived prototypes is not the objective. Centrifugal tests can alleviate the problem of factor (a), but usually not the problem of factor (b), which may become even worse when using models smaller than those used in the 1 g tests.

2.1.1. Conventional type bridge (CB)

The model is a one-span bridge comprising a pair of gravity-type abutments simply supporting a girder via a pair of fixed and movable bearings with unreinforced backfill (Fig. 4(a)). The fixed bearing was a pin, allowing the right end of the girder to rotate, while the movable bearing was a linear-motion bearing, allowing the left end of the girder to slide horizontally. Hence, the dynamic behavior of model CB is un-symmetric with the abutment on the right side being dynamically less stable than the one on the left side.

The model girder that simulates a 20-m-long prototype should be 2 m long. Due to the size constraint of the sand box, a shorter one, 60.8 cm long, 25 kg in weight and made of steel, was prepared. An additional mass of 180 kg was placed at the center so that the horizontal and the vertical loads transmitted to the abutments would become identical to those by a 2-m-long model girder. The model girder was arranged 51 cm above the ground level (i.e., 5.1 m with the prototype). The same model girder was used for all the bridge models. A pair of gravity-type abutments (59 cm wide, 4.5 cm thick times 45 cm high) and its spread-footings (59 cm wide, 20 cm thick times 6 cm high) were made of duralumin. The back faces of the two abutments and the bottom faces of their foundations, which were in direct contact with the backfill and the supporting ground, were made to be rough by being covered with a sheet of sand paper (No. 150) (Fig. 5(d)).

Please cite this article as: Tatsuoka, F., et al., Stability of existing bridges improved by structural integration and nailing. Soils and Foundations (2012), http://dx.doi.org/10.1016/j.sandf.2012.05.004

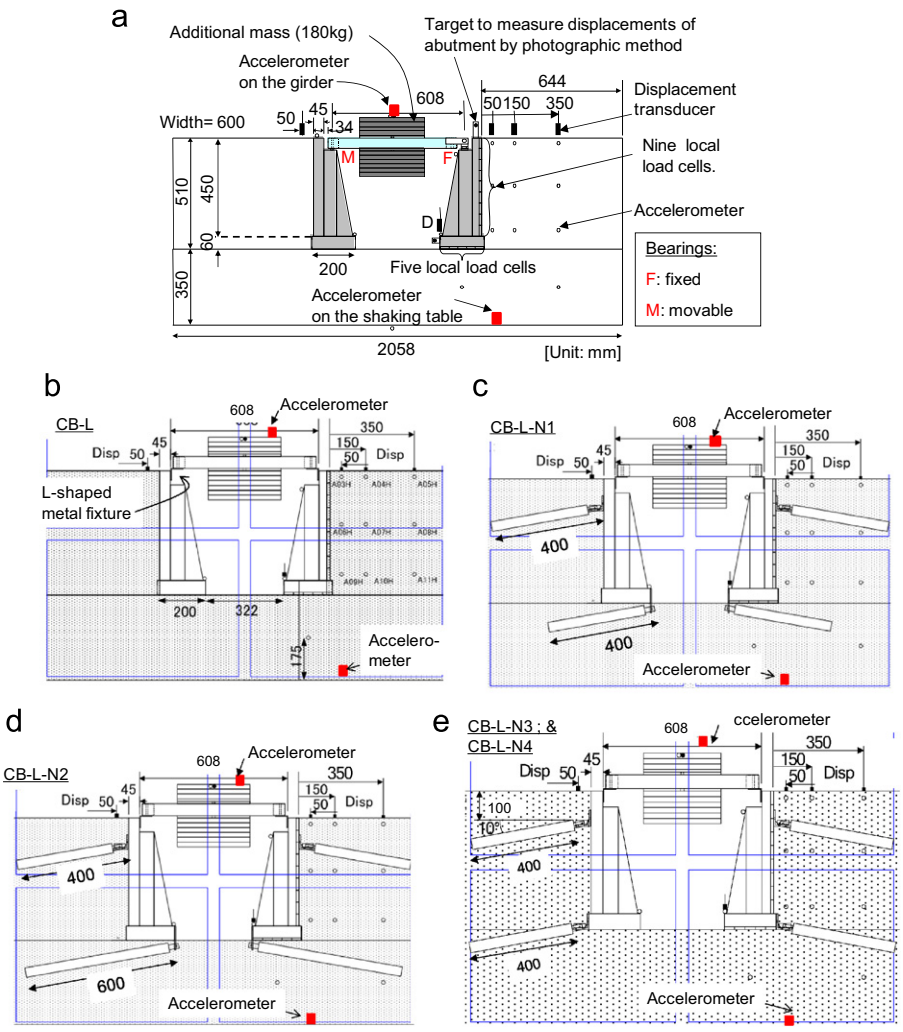

Fig. 4. Shaking table test models: (a) CB; (b) CB-L; and (c–e) NRS integrated bridges (CB-L-N1, CB-L-N2, and CB-L-N3/CB-L-N4). In (b)–(e), only the zone visible through the glass window (Figs. 8–11) is presented. All units are in mm.

The supporting ground and the backfill of this and the other models were produced by pluviating air-dried Toyoura sand ($e_{max}=0.970$, $e_{min}=0.602$, $G_s=2.65$, $U_c=1.64$ and $D_{50}=0.179$ mm) to obtain a relative density D_r of 90%. On the crest of the backfill, a surcharge of 1 kPa, made of lead shots, was placed to simulate the road base for railways or highways. To observe the deformation of the backfill, 7mm-thick horizontal layers of black-dyed Toyoura sand, at a vertical spacing of 10 cm, and a number of small circular targets were placed on the right-hand side abutment and backfill immediately behind the front glass window (as shown in Figs. 8–11). Residual displacements of the abutment after each loading stage were obtained by measuring the displacements at the targets seen in the pictures. This and the other models were densely instrumented, as shown in Fig. 4. Nine local two-component load cells with a load-sensing platen, 13 cm wide and 5 cm high, were arranged at the center of the back of the right-hand side abutment to measure the distributions of vertical shear stress and horizontal normal stress (Figs. 5(c) and (d)). Five similar load cells were also arranged at the bottom face of the abutment footing.

2.1.2. CB-L (Fig. 4(b))

The girder was structurally integrated to a pair of gravity-type abutments of model CB (Fig. 4(a)) by means of a pair of L-shaped metal fixtures (20 cm long, 5 cm wide and 3 mm thick). The peak resisting moment of the fixture is equal to about 0.5 kN m (Tatsuoka et al., 2009). This strength is much smaller than the moment produced by the earth pressure activated on the facing when this bridge model starts failing. Therefore, the bending moment in these fixtures does not become the major resisting component. The backfill was unreinforced air-dried Toyoura sand, as model CB.

2.1.3. CB-L-N1 (Fig. 4(c))

This and the following three are four versions of the NRS integrated bridge. The backfill and a part of the supporting ground of model CB-L (Fig. 4(b)) were nailed using two layers of nails on each side. Each layer comprised two 40-cm-long nails, as shown in Fig. 5(b) (i.e., a total of eight nails for this model). The top nails were connected to the top of the abutment, while the

Please cite this article as: Tatsuoka, F., et al., Stability of existing bridges improved by structural integration and nailing. Soils and Foundations (2012), http://dx.doi.org/10.1016/j.sandf.2012.05.004

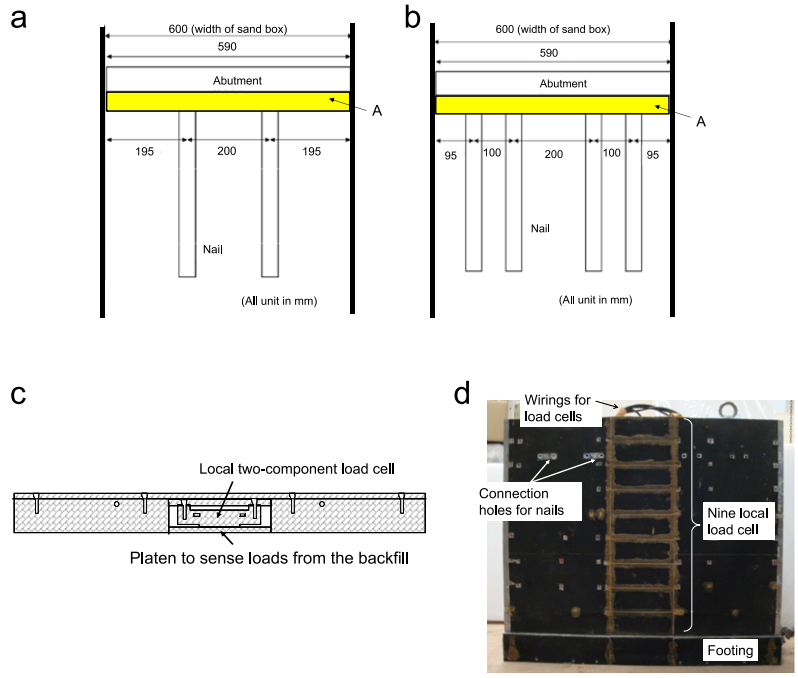

Fig. 5. (a and b) Two or four nails per layer (four only with CB-L-N4), (c) details of part A, and (d) back of the abutment.

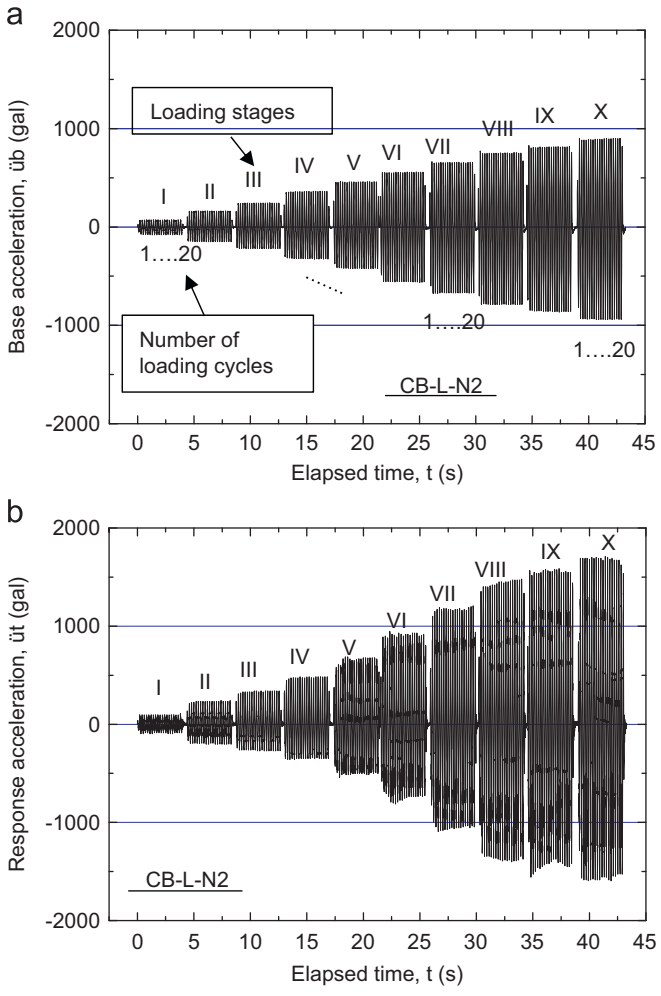

Fig. 6. Time histories of (a) base acceleration at the shaking table and (b) response acceleration at the girder, model CB-L-N2.

bottom nails were connected to the toe of the footing of the abutment via pin connectors so as not to transmit any moment. The model nails were hollow circular brass rods with a diameter of 4 cm; they modeled full-scale large-diameter nails with a diameter of 40 cm based on a length scale factor of $\lambda=10$. The actual nails comprise a central reinforcement rod of steel or FRP covered by soil mixed in-place with cement-slurry (Tateyama et al., 1996). This type of large-diameter nail is often used to reinforce relatively weak soil (typically fills), designed to have a large surface area for sufficient pull-out strength and adequate tensile rupture strength against the design earth pressure. The average density of the model nail is 2.08 g/cm^3 for a length of 40 cm (and 1.95 g/cm^3 for a length of 60 cm used in model CB-L-2 shown below) to simulate the actual nails. The surface of the model nail was made to be rough by gluing Toyoura sand particles to it. A set of electric-resistant strain gauges was attached to the surface of one nail in each layer. In usual practice, full-scale large-diameter nails are installed at an inclination with an angle of -10° from the horizontal in order to retain the cement-mixed soil forming nails in the slurry state inside a bored hole and to ensure that the nails effectively resist against global active failure. The arrangement of the model nails in the present study followed this practice. Prototype nails are installed in the existing backfill. In this study, however, the model backfill was placed after the model nails had been arranged. The possible effects of this difference on the dynamic behavior should be insignificant, as dynamic excitation is an event that occurs far after construction with both prototypes and these model tests.

Please cite this article as: Tatsuoka, F., et al., Stability of existing bridges improved by structural integration and nailing. Soils and Foundations (2012), http://dx.doi.org/10.1016/j.sandf.2012.05.004

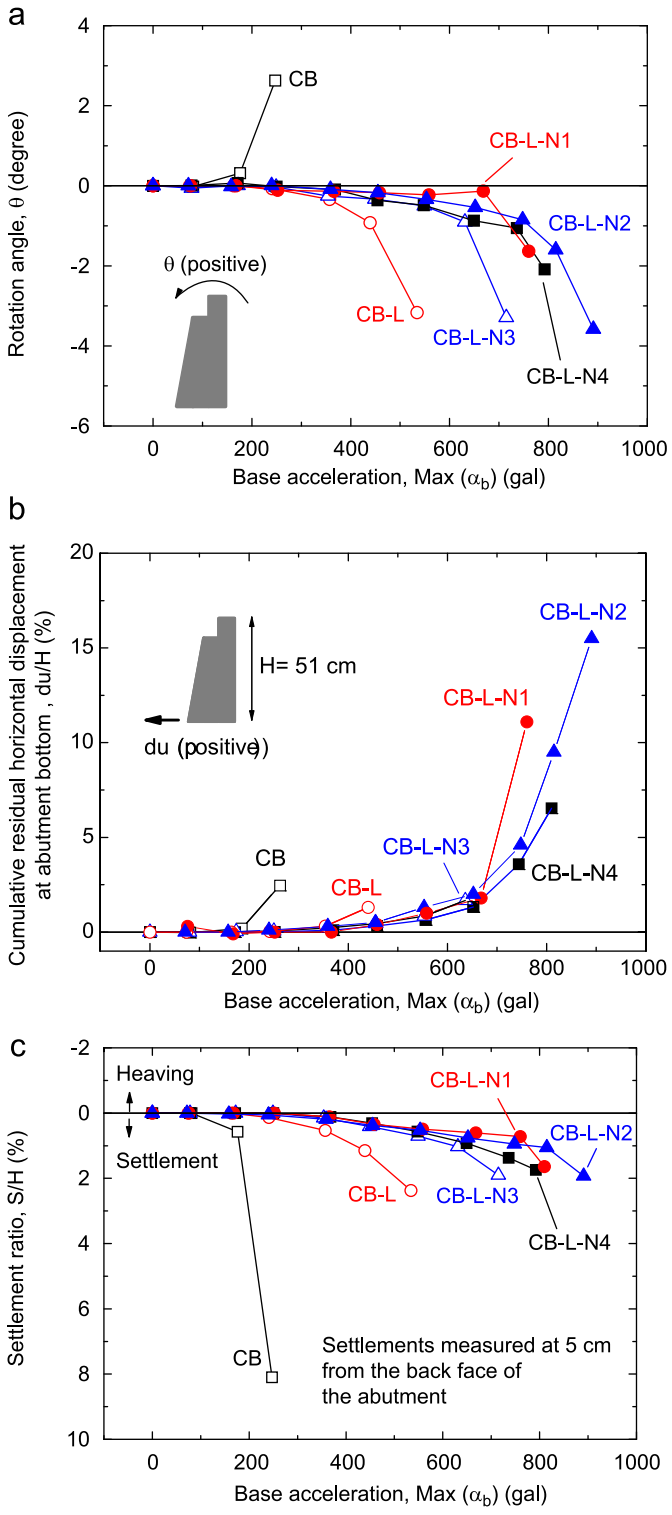

Fig. 7. Residual deformation of six bridge models: (a) rotation of the abutment; (b) lateral displacements at the abutment footing; and (c) settlement at the backfill crest.

2.1.4. CB-L-N2 (Fig. 4(d))

The bottom nails (40 cm long) of model CB-L-N1 were replaced with ones 60 cm long to increase the pull-out strength. This model exhibited the highest dynamic stability among those tested in the present study.

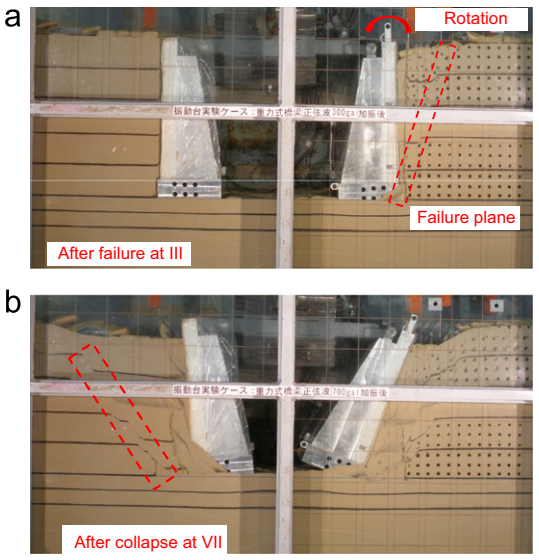

Fig. 8. Model CB at (a) failure at stage III and (b) collapse at stage VII (a rectangular block of broken line denotes the location of a shear band).

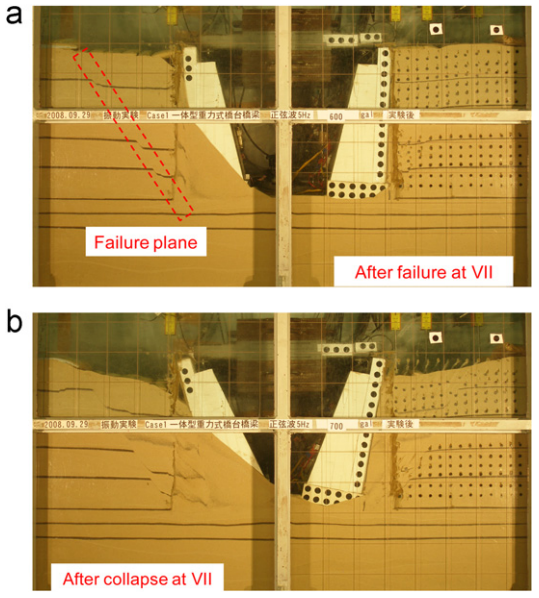

Fig. 9. Model CB-L at (a) failure and (d) collapse.

2.1.5. CB-L-N3 (Fig. 4(e))

The bottom layer nails of model CB-L-N1 were connected to the heel of the abutment footing, which resulted in a lower dynamic stability.

2.1.6. CB-L-N4 (Fig. 4(e))

The number of nails per layer of model CB-L-N3 was increased from two to four in order to increase the pull-out strength (Fig. 5(b)). Thus, a total of 16 nails were used. This arrangement increased the dynamic stability, but the resultant stability was not proportional to the total number of nails.

Please cite this article as: Tatsuoka, F., et al., Stability of existing bridges improved by structural integration and nailing. Soils and Foundations (2012), http://dx.doi.org/10.1016/j.sandf.2012.05.004

2.2. Dynamic loading

The bridge models were subjected to sinusoidal base motion at a fixed frequency of $f_i = 5$ Hz having 20 cycles per stage (Fig. 6(a)). Fig. 6(b) shows the corresponding time history of acceleration recorded at the girder. These are representative of those obtained by the present study.

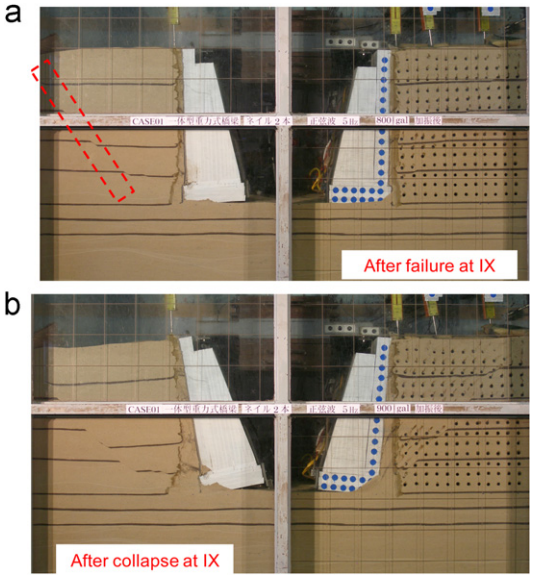

Fig. 10. Model CB-L-N1 at (a) failure and (d) collapse.

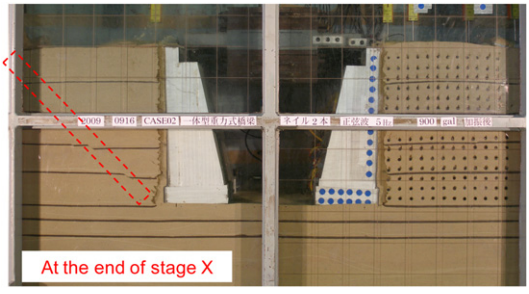

Fig. 11. Model CB-L-N2.

The amplitude of the base acceleration (α_b) was increased stage by stage by a target increment of 100 gal, from 100 gal until the failure or the collapse took place. $f_i = 5$ Hz was selected to be lower than the initial value of the natural frequency (f_0) of the bridge models (listed in Table 1). This was based on the consideration that the initial f_0 value of the full-scale conventional-type bridges simulated in the present study (under undamaged conditions) is higher than typical predominant frequencies of strong earthquake motions ($f_p = 1$–3 Hz). As seen from Table 1, the initial f_0 values of the reinforced conventional-type bridge models (CB-L, CB-L-N1 and CB-L-N2) are higher than the original conventional-type bridge model (CB), thus much higher than $f_i = 5$ Hz.

The results from similar shaking table tests on models of GRS integral and NRS integrated bridges (Muñoz et al., 2012; Tatsuoka et al., in press) showed that the dynamic stability for input frequency f_i, ranging from 2 Hz to 30 Hz, including the one when $f_i = 5$ Hz, can be summarized in a unified way when based on the tuning ratio, $\beta =$ "input frequency f_i"/"transient natural frequency f_0 of a given bridge model". That is, the dynamic behavior when f_i is other than 5 Hz can be inferred from the behavior when $f_i = 5$ Hz when based on this framework.

2.3. Residual displacement and deformation

Figs. 7(a)–(c) show the residual displacements at the right-hand side abutment of the six bridge models (Figs. 4(a)–(e)) observed at the end of the respective loading stages. For a fair comparison, these displacements are plotted against the maximum base acceleration, Max(α_b), at the respective stages, not against the response acceleration, which is different for the same Max(α_b) among these different models. As the amplitude of the base acceleration (α_b) during the respective loading stages was not kept exactly constant, the value of Max(α_b) was selected in these plots. Fig. 7(a) shows the residual rotation of the abutment, positive when the active displacement is larger at the abutment top than at the abutment footing. Fig. 7(b) shows

Table 1
Initial natural frequencies and several physical quantities at the start of failure of four bridge models.

Bridge type	Initial natural frequency, f_0 (Hz)	Physical quantities at the start of failure (i.e. at resonance)						
		Loading stage	(1) $M_{peak} = (6)/(4)$	(2) $\beta_{resonance}$	(3) $\xi_{resonance}$	(4) $(\alpha_b)_{resonance}$ (gal)	(5) Max(α_b) (gal)	(6) Strength $= (\alpha_t)_{resonance}$ (gal)
CB	11	III (5)[a]	1.85	0.97	0.33	214	228	397
		VII (6)[b]	1.43	0.91	0.52	635	659	906
CB-L	25	VII (4)	1.51	0.98	0.45	606	616	932
CB-L-N1	25	IX (20)	1.48	0.86	0.49	793	813	1172
CB-L-N2[c]	25	X (20)	> 1.44	> 0.75	> 0.50	> 885	> 902	> 1277

[a]The numbers in the parenthesis indicate the number of cycle at each loading stage.
[b]The values at the second resonance after the girder has contacted the abutment at a movable bearing.
[c]The resonance was approached but not reached by the end of test.

Please cite this article as: Tatsuoka, F., et al., Stability of existing bridges improved by structural integration and nailing. Soils and Foundations (2012), http://dx.doi.org/10.1016/j.sandf.2012.05.004

the residual horizontal displacement at the abutment footing, positive for active displacements. Fig. 7(c) shows the residual settlement at the crest of the backfill at a distance of 5 cm from the back face of the abutment. Figs. 8–11 show the pictures of models CB, CB-L, CB-L-N1 and CB-L-N2 at failure and at collapse. Here, failure is defined as the start of deformation exceeding a serviceability limit value (as will be described more in detail later) and collapse as the large deformation by which the structure should be extensively repaired or reconstructed to re-open the service. The failure modes of models CB-L-N3 and CB-N-L4, which are similar to those of models CB-L-N1 and CB-L-N2, are not shown here due to page limitations. The following trends may be seen from these figures. Firstly, the dynamic stability of model CB was lowest. Only the abutment of this model exhibited overturning with active movements larger at the top than at the footing (Fig. 8(a)). Yet, the active displacement at the abutment footing (du/H) was also largest. Correspondingly, the settlement in the backfill (S/H) was also largest. Secondly, model CB-L was much more stable with the girder integrated to the abutments. The overturning failure mode disappeared, while the values of du/H (at the abutment bottom) and S/H became much smaller. Thirdly, all the NRS integrated bridge models with nailing (CB-L-N1–N4) were more stable than model CB-L, showing the significant effects of nailing. Among them, the dynamic stability of model CB-L-N2 (using longer bottom nails connected to the toe of the abutment footing) was higher than model CB-L-N1 (using similar but shorter bottom nails). This is due likely to an increase in the pull-out strength of the bottom nails. Fourthly, the dynamic stability of model CB-L-N1 was noticeably higher than model CB-L-N3 (using the same short nails connected to the heel of the abutment footing). This is due likely to the following mechanism. An integrated bridge fails in association with the large rotational displacements of the abutment around its top with large active displacements at its footing. During this process, large upward displacements take place at the toe of the abutment footing, which leads to a separation of the toe of the abutment footing from the supporting ground and a serious loss in abutment stability. This mode of abutment displacement is much more effectively restrained by connecting the nails to the toe of the abutment footing than to the heel. This mechanism was confirmed by smaller cyclic and residual vertical displacements at the toe of the abutment footing with model CB-L-N1 than with model CB-L-N3. Lastly, the dynamic stability of model CB-L-N4 (using four bottom nails per layer connected to the heel of the abutment footing) was noticeably higher than model CB-L-N3 (using two bottom nails per layer connected to the heel of the abutment footing), due likely to an increase in the total pull-out resistance of the nails. However, despite a smaller total volume of nails, model CB-L-N2 (using two bottom nails per layer connected to the toe of the abutment footing) was noticeably more stable than model CB-L-N4. This means that model CB-L-N4 is less cost-effective than model CB-L-N2.

As seen from Figs. 7(c) and 8(a), with model CB, a large bump developed due to active failure in the backfill behind the right-hand side abutment associated with large active displacements at the abutment top. This has taken place very often with full-scale conventional-type bridges by many earthquakes. One of the advantages of the integration of the girder to the abutments with model CB-L (Fig. 4(b)) is a reduction in such bumps in the backfill by making the active displacement at the abutment top very small (Fig. 7(a)). However, because of no nailing, large active displacements may take place at the abutment footing, which induces a large rotation around the abutment top of a large backfill zone (Fig. 9). With nailing, models CB-L-N1 (Fig. 10) and CB-L-N2 (Fig. 11) exhibited much smaller bumps. This feature is a significant advantage of NRS integrated bridges for railways and highways, which allow only a limited number of bumps.

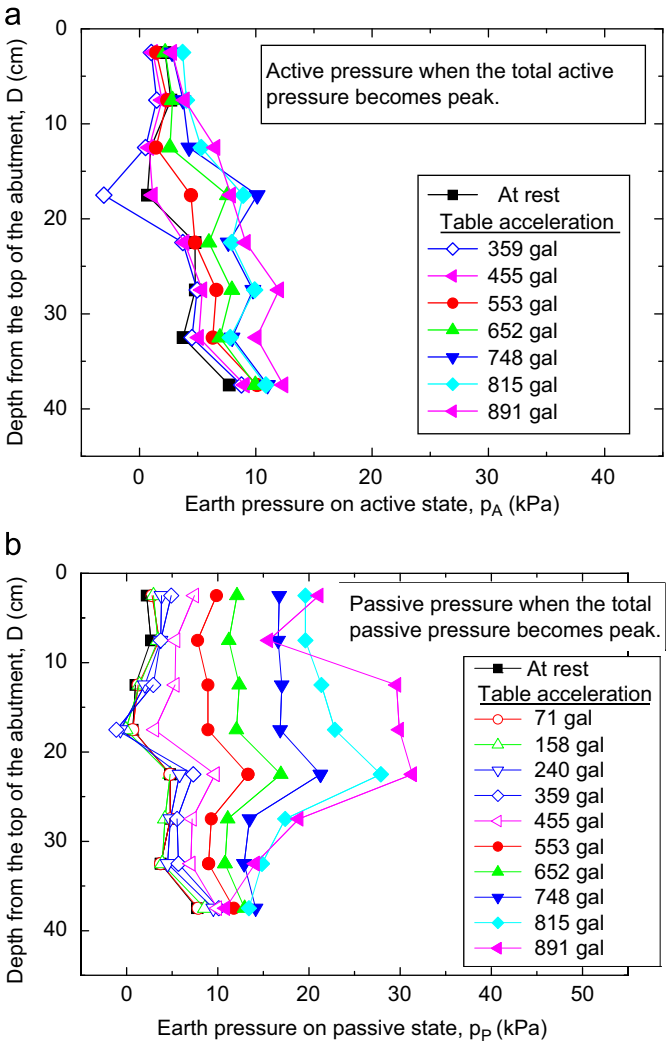

Fig. 12. Lateral earth pressure on the back of the abutment when the total earth pressure is peak at: (a) active state and (b) passive state, model CB-L-N2.

Figs. 12(a) and (b) show vertical distributions of lateral earth pressure on the back of the right-hand side abutment of model CB-L-N2 when the total earth pressure became peak around the moment when the girder displaced most

Please cite this article as: Tatsuoka, F., et al., Stability of existing bridges improved by structural integration and nailing. Soils and Foundations (2012), http://dx.doi.org/10.1016/j.sandf.2012.05.004

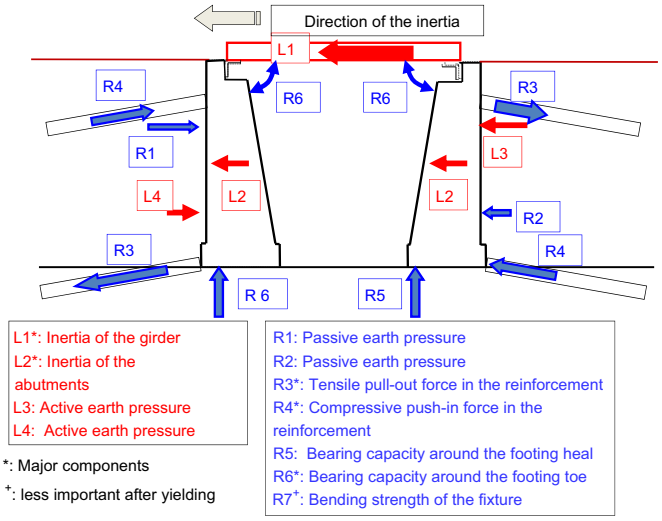

Fig. 13. Load and resistance components for the rotation of the abutment about its top when the right-side abutment is at the active state, NRS integrated bridge.

in the active and the passive directions, like the right- and left-hand side abutments in Fig. 13. In the respective cycles, the largest earth pressure is activated at the passive state (Fig. 12(b)); this trend is stronger at higher levels in the backfill. Such trends indicate that the backfill at upper levels, together with the top nails, resist against the push-in load from the inertia of the abutments and the girder (particularly of the latter) in the passive mode, which becomes more intense as the dynamic load increases. This mechanism was confirmed by axial forces measured in the model nails (not shown here due to page limitations). These test results indicate that the most critical deformation mode leading to failure/collapse for structurally integrated bridges (i.e., models CB-L and CB-L-N1–N4) is the rotation of the abutment around its top with active displacements at its footing. The same failure/collapse mode was observed in the shaking table tests on models of the integral bridge and the GRS integral bridges (Tatsuoka et al., 2009; Muñoz et al., 2012). This mode is triggered by the passive failure of the backfill at higher levels, unlike the active failure mode usually assumed in the aseismic design of ordinary retaining walls. Fig. 13 illustrates the load and resistance components for this critical deformation mode of NRS integrated bridges when the right-hand side abutment is at the active state. Different from GRS integral bridges, compressive forces activated in the nails (denoted as R4) contribute significantly to the dynamic stability.

When the backfill is not reinforced, the likelihood of the occurrence of failure/collapse in this critical mode (Fig. 13) strongly depends on the supporting conditions at the abutment bottom. In the present study, no deep foundation (e.g., piles) was used to highlight the critical failure/collapse mode. When the abutment bottom is fixed to a very stable deep foundation, this model could be effectively restrained. However, it is penalized by high reinforcement costs. Instead, the authors propose to restrain this critical mode by reinforcing the backfill with nails connected to the abutment.

3. Dynamic behavior as a damped SDOF system

3.1. A damped SDOF system

The deformation mode illustrated in Fig. 13 is the first mode of the dynamic behavior of integrated bridges (with and without nailing). The first mode is dominant over the other modes, because this type of bridge is a top-heavy structure with rigid abutments supported by much softer backfill. Hence, to evaluate the significant effects of the structural integration of the girder to the abutments and the nailing on the dynamic stability of the bridge, the four bridge models (CB, CB-L, CB-L-N1 and CB-L-N2) were modeled as a damped single-degree-of-freedom (SDOF) system following the method developed by Shinoda et al. (2003) and extended by Muñoz et al. (2012). Although the dynamic behaviors of models CB-L-N3 and CB-N-N4 are not presented due to page limitations, they can be easily inferred from those of models CB-L-N1 and CB-L-N2 herein reported. The deformation mode of model CB somehow deviated from the one illustrated in Fig. 13 due to an unsymmetrical deformation mode caused by the use of a movable bearing to support only one end of the girder; therefore, the SDOF modeling is less appropriate than the integral bridge models.

Eq. (1) expresses the motion for a damped SDOF system subjected to base acceleration, $\ddot{u}_b$, measured at the shaking table in the present study. The total response acceleration at the mass, $\ddot{u}_t$, measured at the model girder in the present study, is the sum of $\ddot{u}_b$ and the acceleration of the mass relative to the base, $\ddot{u}$ (Eq. (2)).

$$m\ddot{u}_t(t)+c\dot{u}(t)+ku(t)=0 \tag{1}$$

$$\ddot{u}_t=\ddot{u}_b+\ddot{u} \tag{2}$$

where m, k and c are the mass, the stiffness and the coefficient of viscosity of the system and; t is time. The case where $\ddot{u}_b$ is exactly harmonic sinusoidal (Eq. (3)) is herein analyzed.

$$\ddot{u}_b=-\alpha_b \sin(\omega_i t) \tag{3}$$

where α_b is the amplitude of $\ddot{u}_b$. $\ddot{u}_t$ is comprised of the transient response, which is controlled by the initial conditions and decays with time, and the steady-state response (Eq. (4)), which becomes $\ddot{u}_t$ (Eq. (1)) after the transient response dies out.

$$\ddot{u}_t=-\alpha_t \sin(\omega_i t+\varphi)=-\alpha_b M \sin(\omega_i t+\varphi) \tag{4}$$

where α_t is the amplitude of $\ddot{u}_t$, $M=\alpha_t/\alpha_b$ is the magnification ratio of acceleration and φ is the phase difference. As the damping ratio of the bridge models tested in the present study was very high (as shown later), the transient response was recognized only at the first cycle and ignored in the analysis shown below. For the steady-state response,

Please cite this article as: Tatsuoka, F., et al., Stability of existing bridges improved by structural integration and nailing. Soils and Foundations (2012), http://dx.doi.org/10.1016/j.sandf.2012.05.004

the values of M and φ are obtained as

$$M = \sqrt{\frac{1+4\xi^2\beta^2}{(1-\beta^2)^2+4\xi^2\beta^2}} \quad (5)$$

$$\varphi = \arctan\left(\frac{-2\xi\beta^3}{1-(1-4\xi^2)\beta^2}\right) \quad (6)$$

where $\omega_0 = \sqrt{k/m}$ is the natural circular frequency of the system, equal to $2\pi f_0$ (f_0: the natural frequency of the system), ω_i is the input circular frequency, equal to $2\pi f_i$ (f_i: the input frequency), ξ is the damping ratio, equal to $c\omega_0/(2k)$, and β is the tuning ratio, equal to $\omega_i/\omega_0 = f_i/f_0$.

The values of M and φ at each cycle were obtained from a single exact sinusoidal wave fitted to the respective waves of the acceleration recorded at the shaking table and the girder (Fig. 6). From these values for M and φ, the values for β and ξ in each cycle were back-calculated by iteration (i.e., by Newton's method) based on Eqs. (5) and (6). These values for β and ξ represent the transient stiffness and the energy dissipation capacity of the respective bridge models and are the two essential parameters for analysis of the dynamic stability of the bridge models. The increasing process of β associated with a decrease in the stiffness due to the accumulation of damage to the structure by cyclic loading at increasing numbers of loading cycles and acceleration levels is one of the major concerns of this analysis. Table 1 summarizes the initial values for f_0 and several physical quantities observed at the start of failure, which took place at the resonance state, of the four bridge models.

3.2. Four factors of dynamic stability

The dynamic stability of a bridge system is generally controlled by the four factors described as follows.

3.2.1. Dynamic strength

With full-scale bridges, failure is usually defined by the development of (a) deformations and/or displacements of the girder and abutments, (b) structural damage and (c) settlements with bumps in the backfill that exceed specified serviceability limit values. In the present study, the dynamic strength of a bridge model is defined as "the response acceleration at the girder at resonance, $(\alpha_t)_{resonance}$, at which $\beta = \beta_{resonance}$ and M becomes the maximum value, M_{peak}, and the model starts exhibiting significant deformation and displacement (i.e., the start of failure)". $(\alpha_t)_{resonance}$ ($= M_{peak}$ times the base acceleration at resonance, $(\alpha_b)_{resonance}$) was the largest value of the response acceleration (α_t) in the respective model tests. After having passed the resonance state, with an increase in the number of loading cycles (N), the M value started decreasing very quickly from M_{peak} associated with a fast increase in β from $\beta_{resonance}$, caused by a fast decrease in f_0 with a fast increase in the deformation. Finally, collapse took place (i.e., the bridge should be reconstructed or repaired extensively to be used again). The value of α_b varied slightly at respective loading stages (denoted as I, II, III, etc. in Fig. 6(a)), due to changes in the compliance of the shaking table with the model associated with changes in the stiffness of the model. Therefore, in some cases, the maximum of α_b, Max(α_b), was observed during a cycle other than the resonance cycle. The values of $(\alpha_t)_{resonance}$ and $(\alpha_b)_{resonance}$ are listed in Table 1 and plotted in Fig. 14.

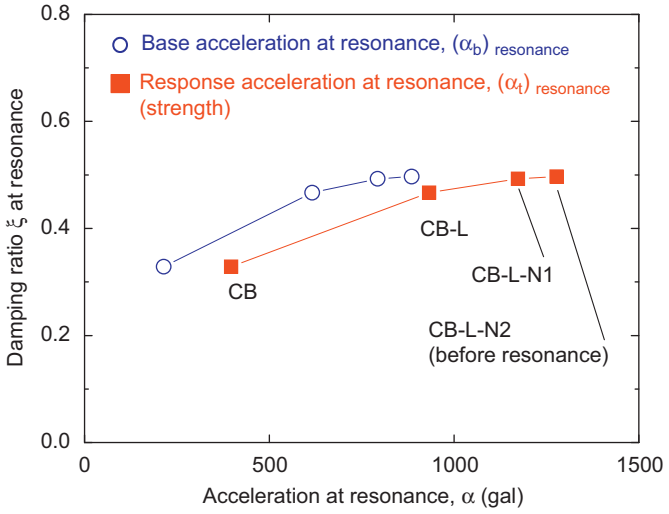

Fig. 14. Relationships between ξ and base and response accelerations at resonance.

In all the shaking table tests reported in this paper, failure started at the resonance state, which was due to such a specific dynamic loading method that the base acceleration (α_b) increased stage by stage at $f_i = 5$ Hz. On the other hand, in similar shaking table tests (Muñoz et al., 2012; Tatsuoka et al., in press), where f_i ranged between 2 and 20 Hz with the initial value of $\beta = f_i/f_0$ still less than unity, when $f_i = 20$ Hz, the resonance state was soon reached before the α_t value became the value at which failure started when $f_i = 5$ Hz, and was quickly passed; therefore, failure did not start.

3.2.2. Initial stiffness

With a given bridge system, as the initial (i.e., undamaged) stiffness becomes larger, the initial value of f_0 becomes larger and the initial value of $\beta = f_i/f_0$, which is less than unity, becomes smaller. Then, the initial value of the magnification ratio of acceleration (M) becomes smaller and the initial response becomes smaller, making the damage to the bridge system smaller, which reduces the possibility of failure during a given loading history.

3.2.3. Dynamic ductility

A higher dynamic ductility means a lower softening rate of bridge system with an increase in the input acceleration level and the number of loading cycles, so a lower speed to reach the resonance state, at which failure may start. When the resonance state is approached, usually the softening rate increases, resulting in a higher chance to reach the resonance state (i.e., for β to become $\beta_{resonance}$) and for

Please cite this article as: Tatsuoka, F., et al., Stability of existing bridges improved by structural integration and nailing. Soils and Foundations (2012), http://dx.doi.org/10.1016/j.sandf.2012.05.004

failure to start. When strong shaking continues after having reached the resonance state, the β value continues increasing and eventually a full collapse may take place. On the other hand, with a sufficiently high dynamic ductility, the β increases only slowly and the resonance state is approached in a delayed manner, keeping the response small and reducing the possibility of failure.

3.2.4. Damping ratio (ξ) at failure

The design response acceleration at the girder (α_t) for a given design earthquake motion is equal to a given design peak horizontal ground acceleration (PGA) times the magnification ratio (M) when PGA takes place. In the present study, the maximum value of α_t is equal to $(\alpha_t)_{resonance} = M_{peak}$ times $(\alpha_b)_{resonance}$ when $\beta = \beta_{resonance}$. The M_{peak} value decreases with an increase in the damping ratio, ξ, at resonance, which tends to increase with an increase in the dynamic strength (i.e., the response acceleration at resonance, $(\alpha_t)_{resonance}$) (Fig. 14).

The dynamic behavior of the four bridge models are evaluated below based on these four factors. It is shown that the integration of the girder, the abutments and the backfill increases all of these factors.

3.3. Overall dynamic behavior of the four models

Fig. 15(a) summarizes the relationships between the amplitudes of the response acceleration at the girder (α_t) and the base acceleration at the shaking table (α_b) in the course of stage by stage increasing α_b at $f_i = 5$ Hz of the four models. Fig. 15(b) shows the relationships between α_t and the back-calculated tuning ratio, $\beta = f_i/f_0$. In these and other similar figures, the results at the first cycle, at which the response is obviously transient, are not plotted. The following trends may be seen from Figs. 15(a) and (b). Firstly, with each model, α_t was not much larger than α_b at the initial stage and α_t became larger than α_b to a greater extent with an increase in α_b. Secondly, the largest α_t took place as β approached unity. After having passed the resonance state, α_t decreased despite the fact that α_b was kept constant. Lastly, among these models, the increasing rate of β with an increase in the number of loading cycles and an increase in α_b decreased with an increase in the dynamic strength (i.e., the value of $(\alpha_t)_{resonance}$). That is, as the dynamic strength increased, the resonance state was reached in a more delayed manner after α_b became larger.

3.4. Dynamic behavior and failure pattern

3.4.1. Conventional type bridge (CB)

Fig. 16(a) shows the relationship between the back-calculated values for M and β at each cycle of model CB, compared with the theoretical relations for several ξ values. Fig. 16(b) shows the corresponding φ–β relations. At the start of stage I, $M = 1.25$ and $\beta = 0.48$. During stages I and II, the β value increased quickly with an increase in the number of cycles (N) and α_b. The φ value increased

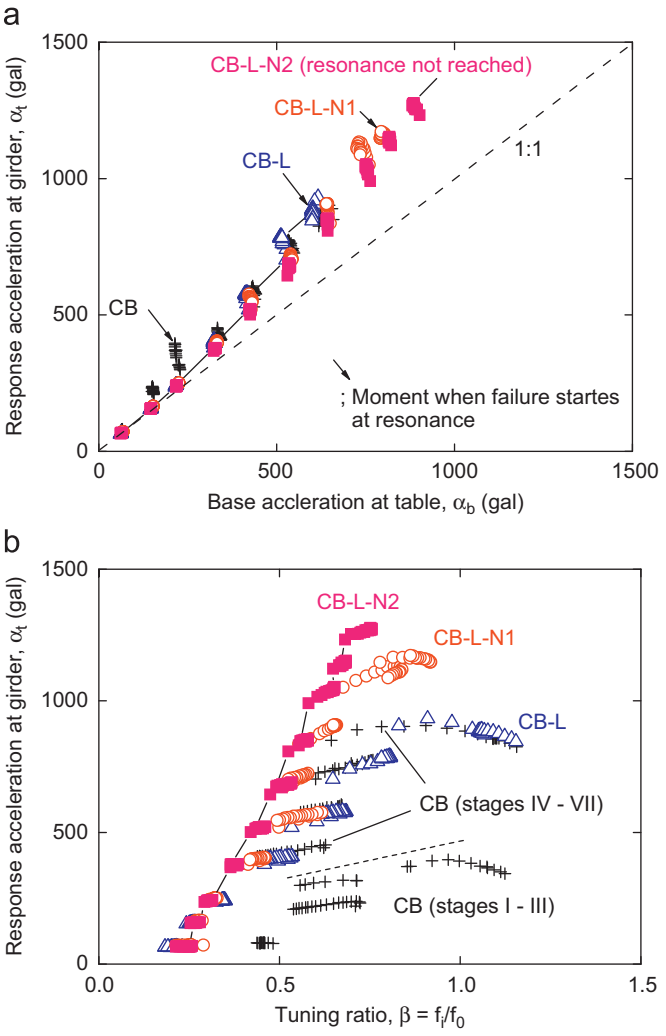

Fig. 15. (a) Response acceleration at the girder vs. base acceleration at the table and (b) response acceleration at the girder vs. tuning ratio, four bridge models ($f_i = 5$ Hz).

from a value close to zero with an increase in the β value. At stage III, the M value increased more quickly with an increase in N corresponding to an increase in the increasing rate of the β value until M became $M_{peak}(=1.85)$, β became $\beta_{resonace}(=0.97)$ and α_b became $(\alpha_b)_{resonance}(=214$ gals) at state III, 5. As seen in Fig. 8(a), at this stage, the right-hand side abutment, supporting the girder via a fixed bearing, started rotating largely around the bottom with larger active displacements at the top with the start of the significant development of shear bands in the active mode in the backfill and significant settlement at the crest of the backfill, in particular immediately behind the abutment. Then, the left end of the girder, supported by a movable bearing, made contact with the top of the abutment after a large sliding at the bearing. As a result, the stiffness of model CB was recovered and the β value decreased to about 0.66 by the end of stage III. Then, the values of β and M at the start of stage IV became similar to their initial values (at the start of stage I). This trend indicates the positive effects of the integration of the girder to the

Please cite this article as: Tatsuoka, F., et al., Stability of existing bridges improved by structural integration and nailing. Soils and Foundations (2012), http://dx.doi.org/10.1016/j.sandf.2012.05.004

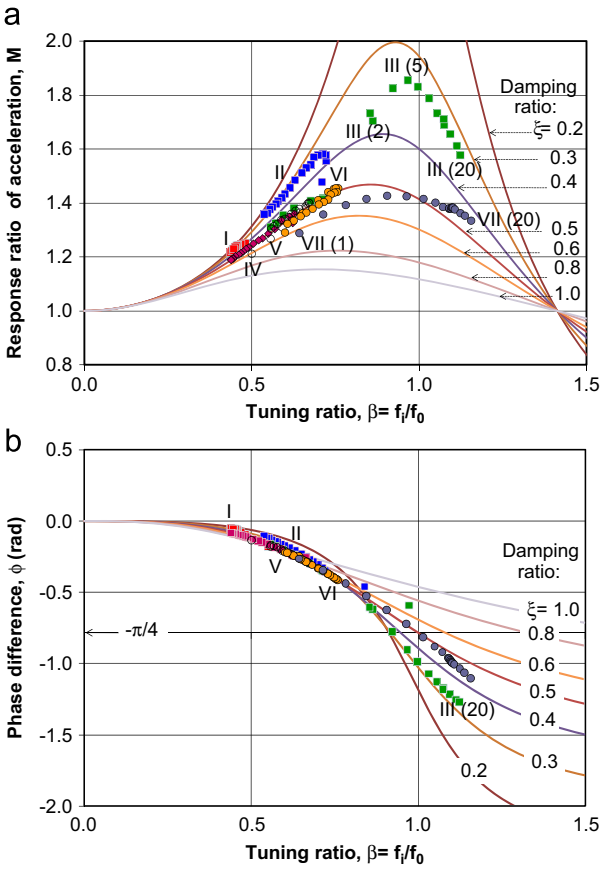

Fig. 16. Dynamic performance of model CB: (a) M–β relation and (b) φ–β relation.

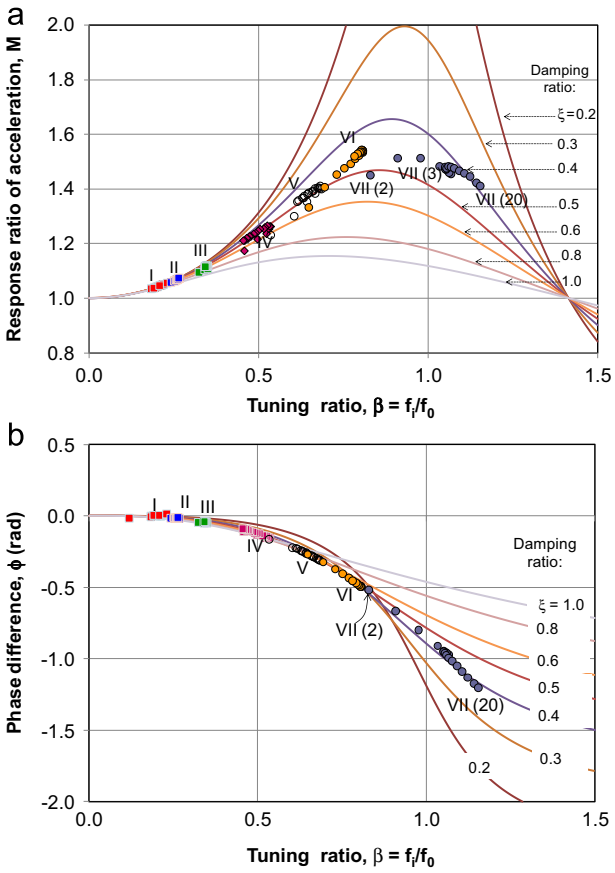

Fig. 17. Dynamic performance of model CB-L: (a) M–β relation and (b) φ–β relation.

abutments on the dynamic behavior of the bridge. At stages IV–VII, the values of M and β increased again in association with the continuous decrease in the stiffness of the bridge system until β became $\beta_{resonace}=0.91$ and M became $M_{peak}=1.43$ at stage VII, where $\mathrm{Max}(\alpha_b)=659$ gals. This second peak, M_{peak}, is significantly smaller than the first peak at stage III. This is due to a significant increase in the ξ value from 0.33 at the first resonance (stage III) to 0.52 at the second resonance (stage VII), caused likely by (i) an increase in the shear strain in the backfill and (ii) an increase in the structural integration by the direct contact of the left end of the girder with the abutment. At stage VII, after having passed the second resonance, the β value increased quickly until a collapse took place (Fig. 8(b)), i.e., the abutments had rotated significantly and their footings had been largely pushed out in association with the development of distinct shear bands in the backfill.

The decrease in stiffness k of the bridge system is due to a decrease in the following factors: (a) the coefficients of sub-grade reaction at the interface between the abutments and the backfill and the supporting ground, (b) the stiffness of the backfill and the supporting ground (in particular, after the shear strength has dropped to the residual value in the shear bands in association with the large active displacements of the abutments), (c) the stiffness of the L-shaped metal connectors between the girder and the abutments (when the girder and the abutments are integrated) and (d) the stiffness at the interface between the nails and the adjacent sand (when the backfill and the supporting ground are nailed). A decrease in the bridge stiffness k may result in progressive failure, and ultimately, collapse. That is, "*a decrease in the bridge stiffness k by degradation of any component accelerates the process of approaching the resonance, which results in further degradation of the components, which accelerates the process toward failure and finally collapse*". Although this process is common with all the bridge models examined in the present study, the approaching rate toward the resonance is largest with model CB; therefore, the stability of model CB is lowest. The movable bearing and the unreinforced backfill are particularly weak components among the whole bridge system. In particular, the girder may dislodge from the movable bearing at low dynamic loads.

3.4.2. *Integrated conventional type bridge (CB-L)*

The M and β values increased from their initial values, $M=1.04$ and $\beta=0.20$ (at the start of stage I) toward the values at the start of failure, $M_{peak}=1.51$ and $\beta_{resonance}=0.98$ when $(\alpha_b)_{resonance}=606$ gals at stage VII (Fig. 17(a)).

Please cite this article as: Tatsuoka, F., et al., Stability of existing bridges improved by structural integration and nailing. Soils and Foundations (2012), http://dx.doi.org/10.1016/j.sandf.2012.05.004

At this stage, the L-shaped metal fixtures started yielding significantly and the abutments started largely rotating around their top with the footing moving forward in association with the development of distinct shear bands in the backfill (Fig. 9(a)). The decrease in the bridge stiffness k in this case is mainly caused by a decrease in factors (a), (b) and (c) (listed above). The process leading to the failure and collapse of model CB-L was substantially slower than model CB. In particular, at stage III (at which model CB started failing), the β value of model CB-L was still 0.37 and the M value was still 1.11. This increase in the dynamic ductility can be attributed to the integration of the girder to the abutments. In the later cycles at stage VII, the transient resonance was passed and the value of M noticeably decreased with an increase in the number of cycles (N) in association with the continuous increase in the values of β and φ. Ultimately, the β value became much larger than unity and the collapse state was reached (Fig. 9(b)), i.e., the abutments had rotated significantly, the L-shaped metal fixtures had yielded significantly and the bottoms of the abutments had been largely pushed out, resulting in a loss of contact between the abutment bottom and the supporting ground, which led to a substantial decrease in the coefficient of sub-grade reaction. All these phenomena should have made the ultimate bridge stiffness very small.

3.4.3. *Integrated conventional type bridge with short bottom nails (CB-L-N1)*

The increasing rates of β, M and φ with an increase in N and α_b became significantly smaller than those of model CB-L, resulting in much smaller values of β and M at the same loading stage (Figs. 18(a) and (b)). That is, model CB-L-N1 behaved in a more ductile way in the process of reaching failure than model CB-L. Failure started at $\alpha_b=(\alpha_b)_{resonance}=793$ gal when β became $\beta_{resonace}=0.86$ and $M_{peak}=1.48$ at stage IX, much later than model CB-L. At this stage, the L-shaped metal fixtures started yielding noticeably and the abutments started noticeably rotating about the top with distinct shear bands developing in the backfill (Fig. 10(a)). The stiffness k of model CB-L-N1 decreased with a decrease in factors (a), (b), (c) and (d). However, due to nailing, the degradation rate of stiffness k substantially decreased; therefore, the increasing rate of β substantially decreased (i.e., the model became much more dynamically ductile). Resonance was reached when $\alpha_b=\mathrm{Max}(\alpha_b)=813$ at stage IX. Then, resonance was passed. Collapse took place by the end of stage IX (Fig. 10(b)). Yet, the increasing rate of β after the resonance was much lower than model CB-L due to the positive effects of nailing.

3.4.4. *Integrated conventional type bridge with long bottom nails (CB-L-N2)*

Although the initial values of β and M were similar to those for model CB-L-N1 (Table 1), the β value increased

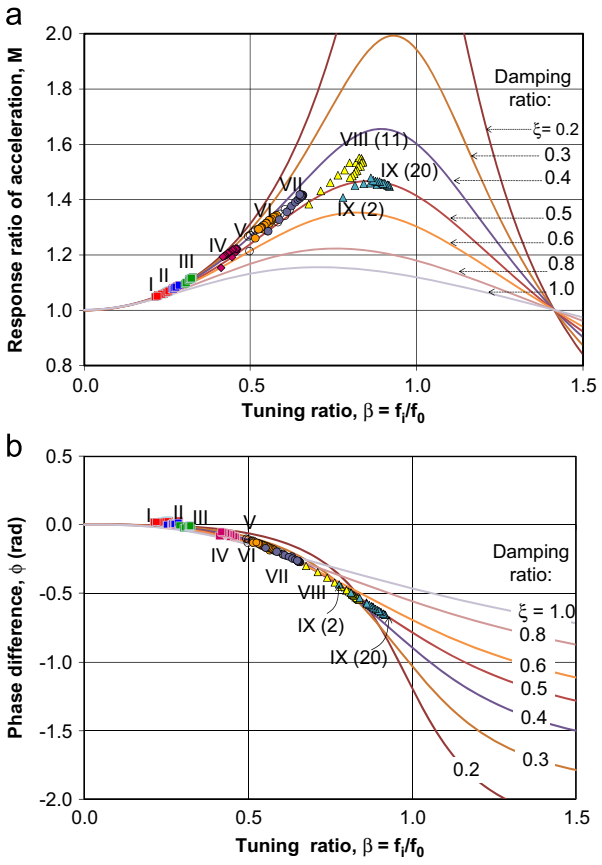

Fig. 18. Dynamic performance of model CB-L-N1: (a) M–β relation and (b) φ–β relation.

at a much lower rate (Figs. 19(a) and (b)). Even at stage X, where α_b was as high as 902 gals, the L-shaped fixtures started yielding only slightly and the abutments started rotating around the top only slightly with some shear bands in the backfill (Fig. 11). The largest $\beta(=0.75)$ and the largest $M(=1.44)$ were observed in the last cycle at stage X (i.e., at X(20) in Figs. 19(a) and (b)). The resonance was not reached by the end of this test. These trends indicate that this model would have been able to withstand another higher loading stage (i.e., stage XI). As model CB-L-N1 failed at stage IX, these results indicate that model CB-L-N2 is dynamically much more stable. This higher performance can be attributed to a decrease in the degradation rate of the bridge stiffness, a higher dynamic strength and a higher damping capacity at failure, all resulting from the use of longer bottom nails connected to the toe of the abutment footings. It is likely that this nail configuration more effectively prevented the uplift of the abutment toe, which, in turn, led to a decrease in the rotation of the abutment around its top with the abutment bottom displacing in the active direction. This trend should have resulted in (i) a smaller yielding rate of the L-shaped metal connectors, (ii) a lower reduction rate of the coefficient of sub-grade reaction at the abutment footing bottom face and (iii) a decrease in the development of shear bands in the backfill.

Please cite this article as: Tatsuoka, F., et al., Stability of existing bridges improved by structural integration and nailing. Soils and Foundations (2012), http://dx.doi.org/10.1016/j.sandf.2012.05.004

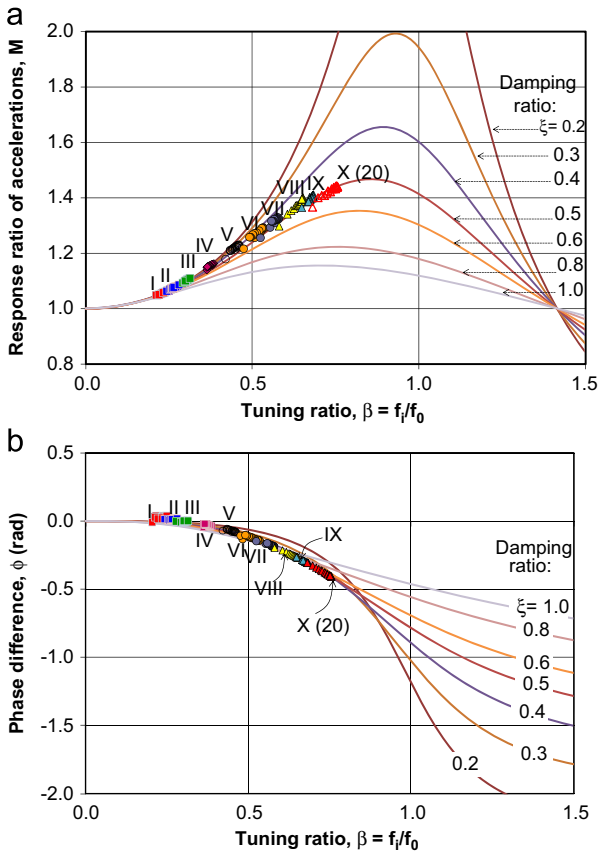

Fig. 19. Dynamic performance of model CB-L-N2: (a) M–β relation and (b) φ–β relation.

3.5. Comparison of dynamic stability based on the four factors

3.5.1. Dynamic strength

Fig. 14 compares the dynamic strengths (i.e., the response acceleration at resonance, $(\alpha_t)_{resonance}$) of the four bridge models. For reference, the base accelerations at resonance, $(\alpha_b)_{resonance}$, are also plotted. The dynamic strength increases consistently by integrating the girder to the abutments (from model CB to model CB-L), then by nailing the backfill and part of the supporting ground with short nails connected to the abutment footing toe (from model CB-L to model CB-L-N1), and finally by using longer bottom nails (from model CB-L-N1 to model CB-L-N2).

3.5.2. Initial stiffness and softening rate

The following are two measures to keep the dynamic state as remote as possible from the resonance by keeping the β value as smaller as possible than the value at resonance: *Measure 1*: making the initial stiffness larger to make the initial value of natural frequency f_0 higher and *Measure 2*: making the decreasing rate of the bridge stiffness smaller to make the decreasing rate of f_0 smaller. If these measures are very effective, the resonance state may not be reached for a given input motion. Figs. 20(a)–(c) show the transient values of (a) β; (b) f_0; and (c) M at each cycle, plotted against the base acceleration (α_b) of the four models. The following trends may be seen. Firstly, the initial value of β (at the start of stage I) of model CB is largest (close to 0.5), while the values of the other three models, CB-L, CB-L-N1 and

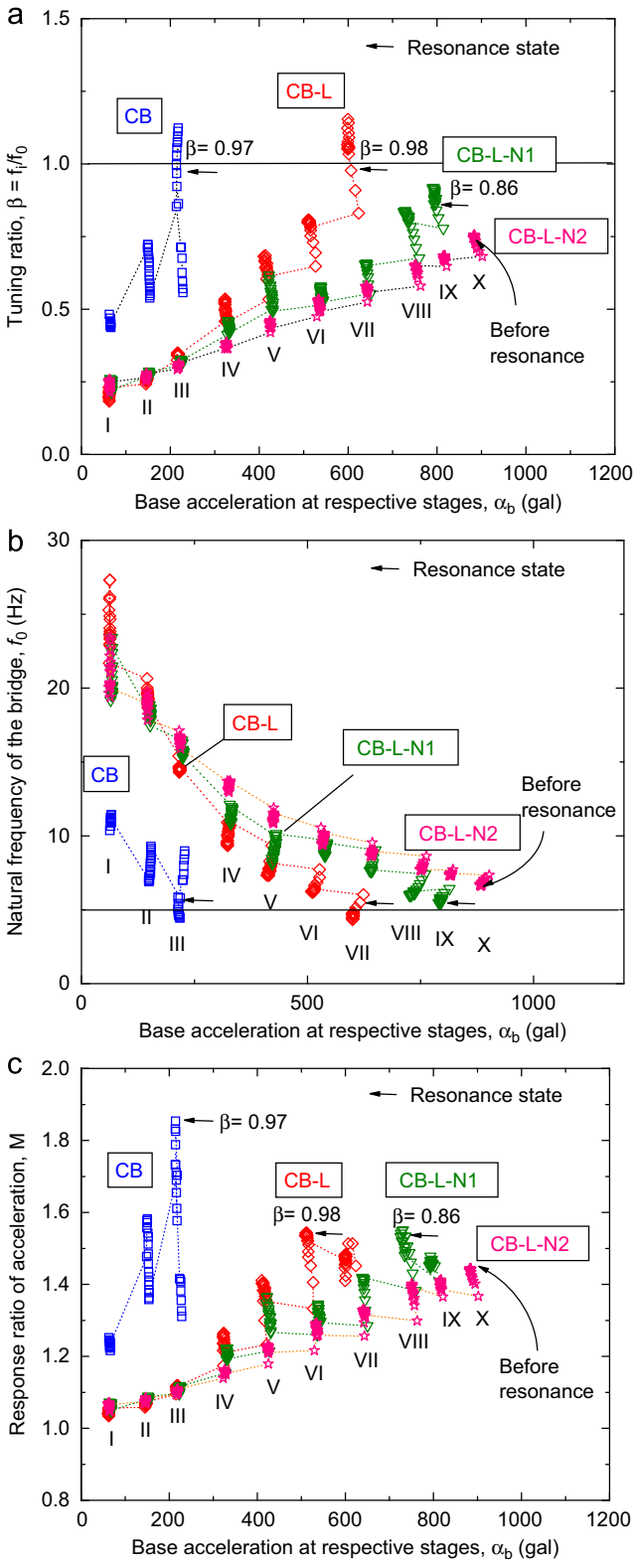

Fig. 20. Relationships between (a) β (b) f_0 and (c) M and α_b at each cycle, four bridge models.

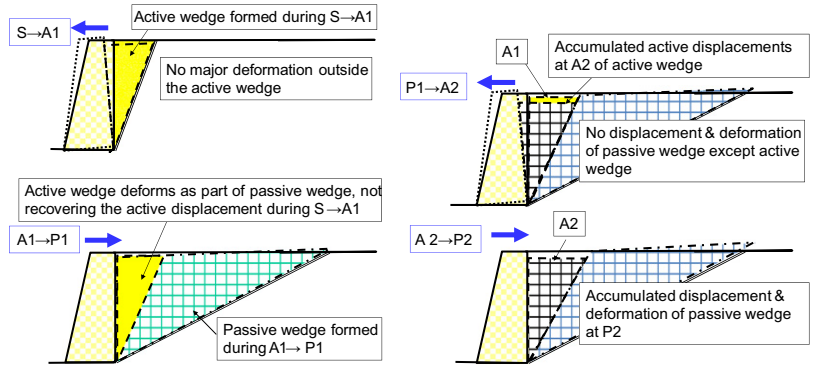

Fig. 21. Dual ratchet mechanism when the abutment bottom is hinged (Tatsuoka et al., 2009, 2010).

CB-L-N2, are similar and much smaller, about 0.20 (Fig. 20(a)). This trend is due to the fact that the initial values of f_0 of models CB-L, CB-L-N1 and CB-L-N2 are similar (about 25 Hz) and much larger than the value of model CB (about 11 Hz) (Fig. 20(b)). These results indicate that the initial stiffness of model CB was effectively increased by integrating the girder to the abutments (i.e., *Measure 1*), whereas nailing was not effective as *Measure 1*. Secondly, the increasing rate of β with an increase in the number of cycles (N) and α_b of model CB-L is much smaller than model CB (Fig. 21(a)). These results indicate that integrating the girder to the abutments is very effective as *Measure 2*. Moreover, the increasing rate of β of model CB-L-N1 became smaller than that of model CB-L after α_b became larger than about 300 gals. These results indicate that, as *Measure 2*, nailing became effective after the deformation of the bridge had become fairly large. In addition, the increasing rate of β with an increase in N and α_b of model CB-L-N2 became smaller than that of model CB-L-N1 when α_b became larger than about 600 gals. These results indicate that, as *Measure 2*, using longer nails connected to the toe of the abutment footing became effective after the lift-up of the toe of the abutment tended to become large when approaching the failure state. Lastly, as a result of the two trends described above, the initial value of $M(=1.25)$ and its increasing rate with N and α_b of model CB were much larger than those of the integrated bridge models (Fig. 20(c)). In addition, the use of nails connected to the toe of the abutment footing, particularly long nails, decreased the increasing rate of M with N and α_b at high α_b values. In short, the highest dynamic stability of model CB-L-N2 can be largely attributed to the largest initial value of natural frequency f_0 and the smallest decreasing rate of f_0 with an increase in the loading cycle and the base excitation level. These features are achieved by integrating the girder to the abutments and nailing as *Measures* 1 and 2.

3.5.3. Damping ratio at resonance

The M_{peak} value decreased from 1.85 (model CB at the first resonance) to 1.51 by integrating the girder to the abutments (model CB-L), further to 1.48 by nailing (model CB-L-N1) and finally to a value less than 1.44 by using longer nails connected to the toe of the abutment footing (model CB-L-N2). This trend is due to an increase in the damping ratio of the bridge system as a SDOF system, ξ, at resonance (Fig. 14). The damping ratio, ξ, is comprised of (i) the material damping of the L-shaped metal connectors (very small), (ii) the material damping of the backfill and the supporting ground as part of a SDOF system, and (iii) the dissipated dynamic energy of the girder and abutments via wave propagation toward the backfill and the supporting ground outside the SDOF system. The highest value of ξ at failure was observed with model CB-L-N2, which results from the following mechanisms. Firstly, the shear strain in the backfill and the supporting ground at the start of failure was largest because the response acceleration at that moment was highest (i.e., the highest dynamic strength). Hence, the material damping ratio of the backfill and the supporting ground could become highest (component ii). Secondly, component (iii) became the most significant due to the highest degree of integration by structural integration of the girder to the abutments and nailing, which kept a good contact of the girder and the abutments with the backfill and the supporting ground. As seen from Figs. 18 and 19, the values for ξ at the resonance of the NRS integrated bridge models are substantially higher than the values of ordinary reinforced concrete structures used in seismic design (of the order of 0.05). This advantageous feature is due to components (ii) and (iii).

In summary, model CB-L-N2 exhibited the highest dynamic stability among the four models. This can be attributed to the highest dynamic strength, the highest initial natural frequency (i.e., the lowest initial value of β), the lowest increasing rate of β and the highest damping ratio ξ at failure. These features are achieved by (i) structural integration of the girder to the abutments and (ii) nailing with the use of two long large-diameter nails connected to the toe of the abutment footing.

4. Static cyclic loading tests

The issue of sufficient long-term serviceability, in addition to high seismic stability when constructed in a high-seismic zone, is discussed in this chapter.

Please cite this article as: Tatsuoka, F., et al., Stability of existing bridges improved by structural integration and nailing. Soils and Foundations (2012), http://dx.doi.org/10.1016/j.sandf.2012.05.004

4.1. Dual ratchet mechanism

Conventional-type bridges usually use movable bearings to accommodate seasonal longitudinal thermal deformation of the girder. On the other hand, with conventional-type integral bridges and NRS integrated bridges, the thermal deformation of the girder results in cyclic lateral displacements at the top of the abutments, which may cause the development of high passive earth pressure on the back of the abutment and may induce active failure with large settlements in the backfill. Tatsuoka et al. (2009, 2010) showed that these detrimental phenomena are caused by "the dual ratchet mechanism", illustrated in Fig. 21. *Process* $S \rightarrow A1$: Small active failure with the development of an active wedge by a small active displacement of the abutment. *Process* $A1 \rightarrow P1$: The active sliding that has taken place at process $S \rightarrow A1$ is not recovered by this small passive displacement of the abutment, because the passive deformation of the passive wedge zone take places more easily, despite a much larger wedge size. The active wedge deforms in the passive mode as part of the passive zone. *Process* $P1 \rightarrow A2$. By the second small active displacement of the abutment, the active sliding is re-activated, while the part outside the active wedge in the passive zone does not deform. *Process* $A2 \rightarrow P2$: By the second small passive displacement of the abutment, again, the active sliding is not re-covered, while the passive deformation develops further. These processes are repeated during a given lifetime. Although it is small in each cycle, the active sliding accumulates with cyclic loading (i.e., the active ratchet mechanism) and the accumulated active sliding may soon reach the value at which active failure takes place during monotonic active loading. Although it is also small in each cycle, the passive strain in the passive zone accumulates with cyclic loading, which gradually increases the passive earth pressure (i.e., the passive ratchet mechanism). Heaving may take place in the backfill by cumulative passive deformation of the passive zone. As the passive displacement of the abutment when the passive failure takes place during monotonic passive loading is very large, the active failure takes place far before the passive failure takes place during cyclic loading. At the crest of the backfill, large settlement occurs in association with an active failure in the backfill. The actual settlement that takes place in the backfill during cyclic lateral loading is a summation of the settlement due to the dual ratchet mechanism and the settlement by cumulative compressive volumetric strain in the backfill taking place by cyclic straining. These problems with newly constructed integral bridges can be alleviated by reinforcing the backfill with geogrid layers connected to the abutment (Tatsuoka et al., 2009). It is shown below based on model test results that the nailing of the backfill and the supporting ground is also effective for alleviating these problems with integrated bridges.

4.2. Model test method

As the test method is basically the same as the one reported in detail by Tatsuoka et al. (2009) and the one for the shaking table tests described above, only a brief description is given below. The abutment models (39 cm wide, 3.5 cm thick, 48 cm high and made of duralumin) with nails (Fig. 22(a)) and those without nails were constructed inside a sand box (180 cm long × 40 cm

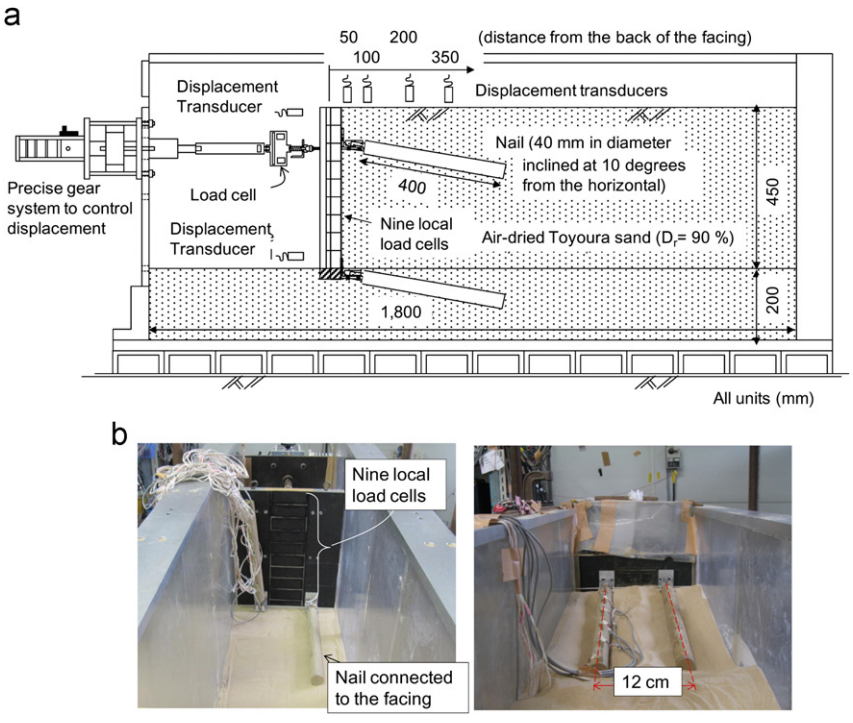

Fig. 22. Static lateral cyclic loading tests on an abutment model with nails in the backfill and supporting ground: (a) general set-up and (b) arrangement of nails.

Please cite this article as: Tatsuoka, F., et al., Stability of existing bridges improved by structural integration and nailing. Soils and Foundations (2012), http://dx.doi.org/10.1016/j.sandf.2012.05.004

wide × 80 cm high). To highlight the effects of nailing, the abutment models were embedded only to a depth of 3 cm in the supporting ground, simulating prototype abutments not supported with any pile foundation. The backfill and the supporting ground were made in the same way as in the shaking table tests (Fig. 4). Two nails were attached to the top and the bottom of the abutment via pin connectors at a horizontal center-to-center spacing of 12 cm (Fig. 22(b)). The models were instrumented at relevant locations to monitor displacements, load and pressure levels (Fig. 22(a)). The abutment was equipped with nine local load cells and the back face was made to be rough.

The top of the abutment model was cyclically and laterally displaced by means of a precise gear-type loading device (Tatsuoka et al., 1994) until the number of cycles (N) became 200, or sooner if the displacement of the abutment became very large. For the active failure in the backfill to take place more easily, the first displacement of the abutment was in the active direction with the subsequent cyclic displacements only at the active side of the original location. The lateral displacement rate at the abutment top was 0.004 mm/s. The ratio of the double amplitude of lateral displacement at the abutment top (D) to the abutment height ($H=48$ cm), D/H, was 0.2%, 0.4% and 0.6%. These values of D/H are realistic for ordinary full-scale integrated bridges (Tatsuoka et al., 2009).

4.3. Test results

Fig. 23 shows the unreinforced backfill and the part of the supporting ground at the end of cyclic loading in three tests performed at three different values of D/H. Fig. 24 shows the nailed backfill and the part of the supporting ground at the same values for D/H. Fig. 25(a) and (b) show the relationships between the total earth pressure coefficient, $K=2Q/(\gamma H^2)$, and the ratio of the lateral displacement at the abutment top (d: positive in the active direction) to the wall height ($H=48$ cm) at different numbers of loading cycles, N, when $D/H=0.6\%$. The backfill and the supporting ground was either unreinforced or nailed. Here, Q is the measured total earth pressure per width and γ is the unit dry weight of the backfill ($=1.60$ gf/cm^3 for $D_r=90\%$). The data when $D/H=0.2\%$ and 0.4% are basically similar to those presented in Fig. 25. Fig. 26(a) and (b) show the relationships between the peak value of K in each cycle (attained when d has returned to zero), K_{peak}, and N for different D/H values when the backfill and the supporting ground was either unreinforced or nailed. Fig. 27(a) compares the relationships between the settlement ratio, S/H, at 5 cm from the back face of the abutment and N. The

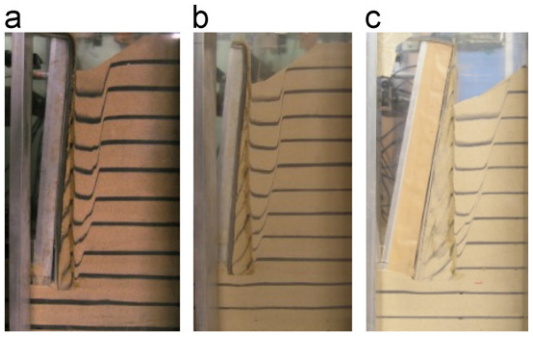

Fig. 23. Active failure in the un-nailed backfill when the abutment bottom is not hinge-supported: (a) after 200 cycles of $D/H=0.2\%$; (b) after 92 cycles of $D/H=0.4\%$; and (c) after 90 cycles of $D/H=0.6\%$ ($H=48$ cm).

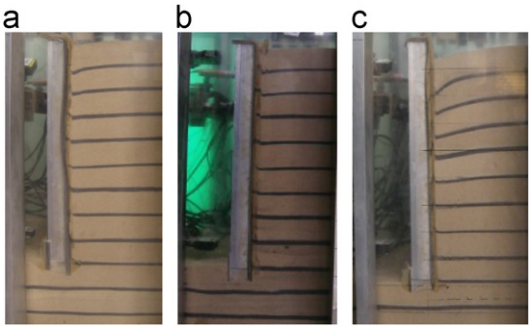

Fig. 24. Active zone in the nailed backfill when the abutment bottom is not hinge-supported: (a) after 200 cycles of $D/H=0.2\%$; (b) after 200 cycles of $D/H=0.4\%$; and (c) after 200 cycles of $D/H=0.6\%$ ($H=48$ cm).

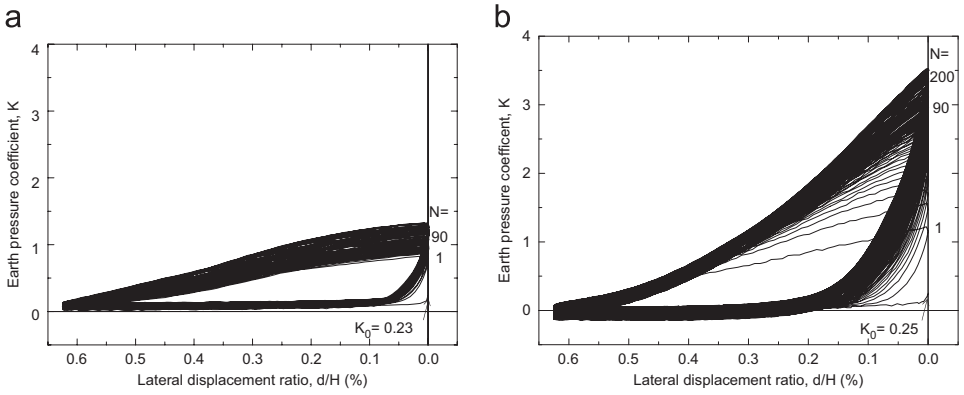

Fig. 25. Relationships between K and d/H at the abutment top when $D/H=0.6\%$ ($H=48$ cm): (a) un-nailed and (b) nailed.

Please cite this article as: Tatsuoka, F., et al., Stability of existing bridges improved by structural integration and nailing. Soils and Foundations (2012), http://dx.doi.org/10.1016/j.sandf.2012.05.004

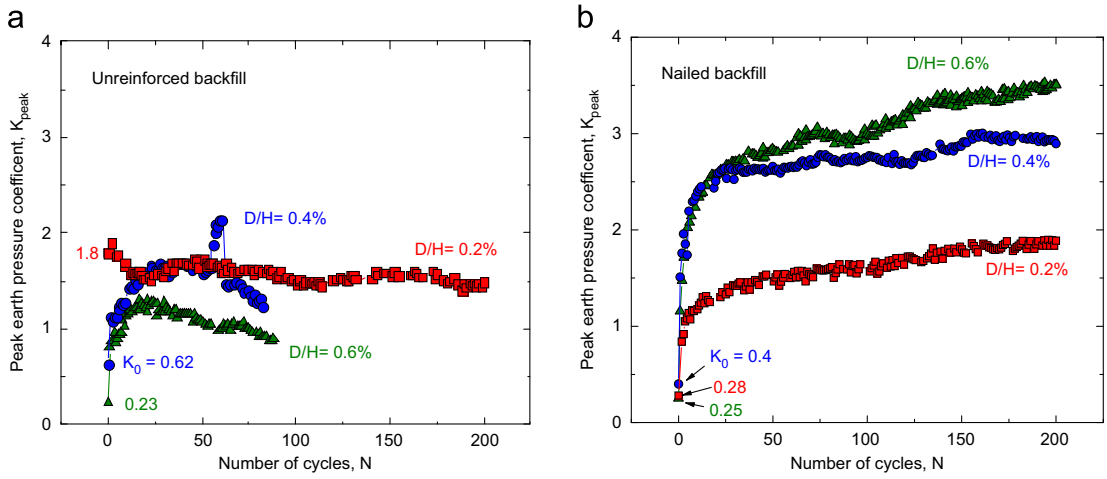

Fig. 26. Variation of peak total earth pressure coefficient with the number of cycle: (a) un-nailed and (b) nailed.

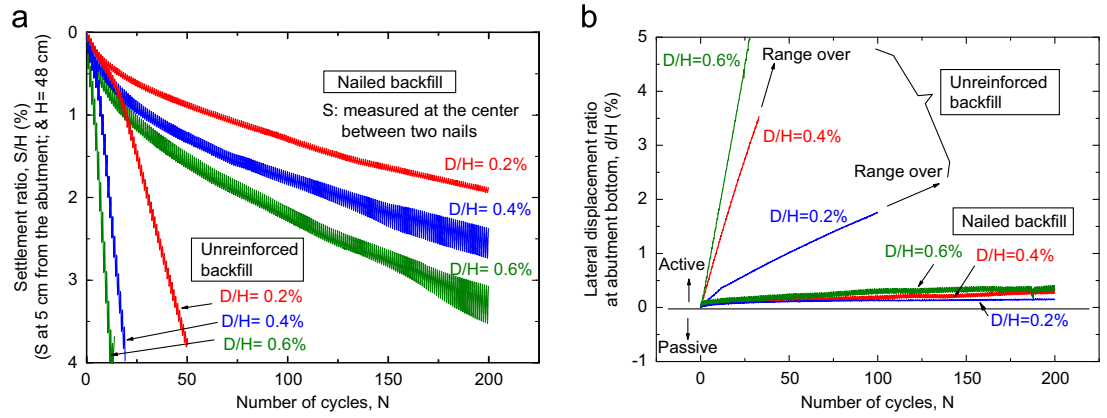

Fig. 27. Relationships between (a) settlement ratio and (b) lateral displacement ratio at the abutment bottom and the number of cycle when the backfill and supporting ground is un-nailed and nailed ($H=48$ cm).

maximum measurable value of S/H was about 4%, determined by a maximum capacity, 20 mm, of the displacement laser sensor used. Fig. 27(b) compares the relationships between the lateral displacement ratio at the abutment bottom, d/H, and N. The following trends may be seen from these results. Firstly, when the backfill was unreinforced, distinct active failure took place in the backfill with very large settlements, even when D/H was as small as 0.2%. In addition, due to the development of large passive earth pressure, the abutment bottom was largely pushed out, which restrained the development of high passive earth pressure. These trends became more significant with an increase in D/H. Secondly, by nailing, the active displacement at the abutment footing became essentially zero. As a result, the active failure in the backfill was effectively restrained and the settlement in the backfill became much smaller. On the other hand, high passive pressure developed because the dual ratchet mechanism was still somehow active despite the nailing. However, this nailing prevented the development of distinct active failure in the backfill, which made the activation of the dual ratchet mechanism much weaker.

In summary, when the girder is integrated to the abutments, the abutment and the backfill can become very stable against cyclic lateral displacements caused by seasonal thermal expansion and contraction of the girder by the use of nails connected to the top and the bottom of the abutment.

5. Conclusions

From the results of model tests and analysis shown above, the following conclusions can be derived:

(1) The seismic stability of existing conventional-type bridges, comprising a girder simply supported by a pair of abutments via a pair of movable and fixed bearings, increases substantially by nailing the backfill and the supporting ground with large-diameter nails connected to the top and the bottom of the abutments and then integrating the girder to the abutments.
(2) The increase in seismic stability is due to (i) an increase in the dynamic strength against response acceleration, (ii) an increase in the initial value of the natural frequency (f_0) of the bridge system to a value sufficiently higher than the predominant frequencies (f_p) of major earthquakes, thereby decreasing the initial response acceleration,

Please cite this article as: Tatsuoka, F., et al., Stability of existing bridges improved by structural integration and nailing. Soils and Foundations (2012), http://dx.doi.org/10.1016/j.sandf.2012.05.004

(iii) a decrease in the decreasing rate of f_0 with an increase in the base acceleration and the number of loading cycles (i.e., an increase in the dynamic ductility), which keeps the f_0 value much higher than the f_p value and keeps the response of the bridge remote from the resonance and (iv) an increase in the damping capacity, which reduces the dynamic response.

(3) The integration of the girder to the abutments results in cyclic lateral displacements at the abutment top by seasonal thermal expansion and contraction of the girder. By the dual ratchet mechanism, significant active failure with large settlements may take place in the backfill, while significant passive earth pressure may develop at the back of the abutment. These detrimental effects can be effectively alleviated by the use of large-diameter nails connected to the top and the bottom of the abutment.

(4) These advantageous features of nail-reinforced soil (NRS) integrated bridges are basically the same as geosynthetic-reinforced soil (GRS) integral bridges for new construction.

Acknowledgments

This study was financially supported by the Ministry of Education, Culture, Sports, Science and Technology, the Japanese Government, the Japan Society for the Promotion of Science and Tokyo University of Science. The shaking table tests were performed at the Railway Technical Research Institute, Japan. The financial support given to the second author, in order to complete his Master course study at Tokyo University of Science, was provided by the Inter-American Development Bank (IDB) through the Japan-IDB Scholarship Program and is gratefully acknowledged. The authors also thank all their previous and current colleagues for their help.

References

Muñoz, H., Tatsuoka, F., Hirakawa, D., Nishikiori, H., Soma, R., Tateyama, M., Watanabe, K., 2012. Dynamic stability of geosynthetic-reinforced soil integral bridge. Geosynthtetics International 19 (1), 11–38.

Shinoda, M., Uchimura, T., Tatsuoka, F., 2003. Improving the dynamic performance of preloaded and prestressed mechanically reinforced backfill by using a ratchet connection. Soils and Foundations 43 (2), 33–54.

Shiranita, K., Tateyama, M., Kouda, M., Kojima, K., Watanabe, K., 2010. A proposal of a method to prolonging the life of exisiting bridge by integrating the girder, abutment and backfill. In: Proceedings of the 45th Japan Conference on Geotechnical Engineering, JGS, Matsuyama, Paper No. 697, pp. 1393–1394 (in Japanese).

Siddiquee, M.S.A., Tanaka, T., Tatsuoka, F., Tani, K., Morimoto, T., 1999. Numerical simulation of the bearing capacity of strip footing on sand. Soils and Foundations 39 (4), 93–109.

Suga, M., Kuriyama, R., Tateyama, M., Kouda, M., Sugimoto, I., Kobayashi, Y., 2011. Reinforcing method of bridge by integration of steel girder, abutment and backfill. In: Proceedings of the 46th Japan Conference on Geotechnical Engineering, JGS, Kobe, Paper No. H-06, pp. 1499–1500 (in Japanese).

Tateyama, M., Tarumi, H., Fukuda, A., 1996. Development of a large diameter short reinforced anchor by cement-mixing method. Grouting and deep mixing. In: Proceedings of the Second International Conference on Ground Improvement Geosystems, Tokyo, pp. 759–765.

Tatsuoka, F., 1992. Roles of facing rigidity in soil reinforcing. Keynote lecture. In: Ochiai et al. (Eds.), Proceedings of the Earth Reinforcement Practice, IS-Kyushu '92, vol. 2, pp. 831–870.

Tatsuoka, F., 2001. Impacts on geotechnical engineering of several recent findings from laboratory stress–strain tests on geomaterials. In: Correia, Brandle (Eds.), 2000 Burmister Lecture, Geotechnics for Roads, Rail Tracks and Earth Structures. Balkema, pp. 69–140.

Tatsuoka, F., Okahara, M., Tanaka, T., Tani, K., Morimoto, T., Siddiquee, M.S.A., 1991. Progressive failure and particle size effect in bearing capacity of a footing on sand. In: Proceedings of the ASCE Geotechnical Engineering Congress, 1991, Boulder, ASCE Geotechnical Special Publication, vol. 27, pp. 788–802.

Tatsuoka, F., Sato, T., Park, C.-S., Kim, Y.-S., Mukabi, J.N., Kohata, Y., 1994. Measurements of elastic properties of geomaterials in laboratory compression tests. Geotechnical Testing Journal, ASTM 17 (1), 80–94.

Tatsuoka, F., Tateyama, M., Uchimura, T., Koseki, J., 1997. Geosynthetic-reinforced soil retaining walls as important permanent. Structures, Mercer Lecture, Geosynthetic International 4 (2), 81–136.

Tatsuoka, F., Tateyama, M., Aoki, H., Watanabe, K., 2005. Bridge abutment made of cement-mixed gravel backfill. In: Indradratna, Chu (Eds.), Ground Improvement, Case Histories. Elesevier Geo-Engineering Book Series, vol. 3. Elesevier Geo-Engineering Book Series, pp. 829–873.

Tatsuoka, F., Hirakawa, D., Nojiri, M., Aizawa, H., Nishikiori, H., Soma, R., Tateyama, M., Watanabe, K., 2009. A new type integral bridge comprising geosynthetic-reinforced soil walls. Geosynthetics International 16 (4), 301–326.

Tatsuoka, F., Hirakawa, D., Nojiri, M., Aizawa, H., Nishikiori, H., Soma, R., Tateyama, M., Watanabe, K., 2010. Closure to discussion on "A new type of integral bridge comprising geosynthetic-reinforced soil walls". Geosynthtetics International 17 (4), 1–12.

Tatsuoka, F., Kuroda, T., Tateyama, M. Research and practice of GRS integral bridges. In: Proceedings of the EuroGeo 5, 2012, Valencia, September, in press.

Watanabe, K., 2011. Application of GRS integral bridge technology to Hokkaido High-Speed Train Line (Shinkansen). Journal of Japan Railway Civil Engineering Association 49 (10), 83–86 (in Japanese).

Please cite this article as: Tatsuoka, F., et al., Stability of existing bridges improved by structural integration and nailing. Soils and Foundations (2012), http://dx.doi.org/10.1016/j.sandf.2012.05.004